
This is an electronic reprint of the original article.
This reprint may differ from the original in pagination and typographic detail.

Isakov, Kirill; Kauppinen, Christoffer; Franssila, Sami; Lipsanen, Harri

Superhydrophobic Antireflection Coating on Glass Using Grass-like Alumina and Fluoropolymer

Published in:
ACS applied materials & interfaces

DOI:
[10.1021/acsami.0c12465](https://doi.org/10.1021/acsami.0c12465)

Published: 04/11/2020

Document Version
Publisher's PDF, also known as Version of record

Please cite the original version:
Isakov, K., Kauppinen, C., Franssila, S., & Lipsanen, H. (2020). Superhydrophobic Antireflection Coating on Glass Using Grass-like Alumina and Fluoropolymer. *ACS applied materials & interfaces*, 12(44), 49957-49962. <https://doi.org/10.1021/acsami.0c12465>

This material is protected by copyright and other intellectual property rights, and duplication or sale of all or part of any of the repository collections is not permitted, except that material may be duplicated by you for your research use or educational purposes in electronic or print form. You must obtain permission for any other use. Electronic or print copies may not be offered, whether for sale or otherwise to anyone who is not an authorised user.

Superhydrophobic Antireflection Coating on Glass Using Grass-like Alumina and Fluoropolymer

Kirill Isakov,* Christoffer Kauppinen, Sami Franssila, and Harri Lipsanen



Cite This: *ACS Appl. Mater. Interfaces* 2020, 12, 49957–49962



Read Online

ACCESS |



Metrics & More



Article Recommendations

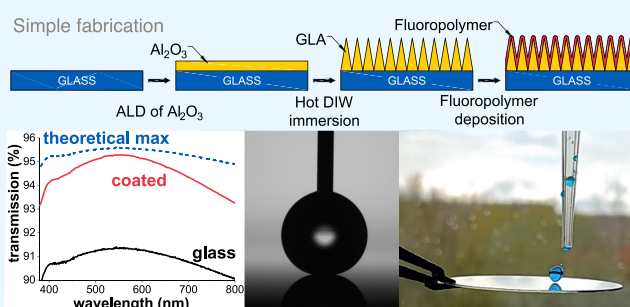


Supporting Information

ABSTRACT: This work presents a superhydrophobic antireflective (AR) coating on glass. The coating consists of a grass-like alumina layer capped with plasma-deposited fluoropolymer. The grass-like alumina is formed by hot water treatment of atomic layer-deposited alumina on glass, and the fluoropolymer is plasma-deposited from CHF_3 . Excellent broadband AR performance is observed in the visible spectrum with an average transmission of 94.9% for single-sided coated glass, which is close to the maximum 95.3% possible for this glass. Extremely desirable contact angles are obtained with 5–7 min-long fluoropolymer treatments on grass-like alumina with 173° advancing and 160° receding contact angles. This type of multifunctional coating can be beneficial in a multitude of applications like self-cleaning AR coating for solar panels, windows in high-rise buildings, sensors, and aerospace applications as well as just utilizing the excellent water repellent behavior in applications where only superhydrophobicity is required.

KEYWORDS: antireflective coating, optical coating, superhydrophobic, self-cleaning, atomic layer deposition, nanostructures

Superhydrophobic anti-reflective coating



1. INTRODUCTION

Antireflective coatings (ARCs) are an important and very common part of the surrounding technology, but multifunctional coatings such as self-cleaning or antisoiling ARCs are not widely adopted. Self-cleaning ARCs can be advantageous in solar energy production, by increasing collected energy and reducing maintenance requirements, as well as in optical sensors and cameras. Self-cleaning and antisoiling properties can be found in superhydrophobic coatings.^{1–7} In such coatings, the antisoiling mechanism is achieved primarily by dust herding,⁷ while one of the main mechanisms of self-cleaning is self-propelled jumping of water droplets.³ In addition, superhydrophobic coatings can act as moisture and corrosion barriers.^{8–10}

The most common and successful way to achieve a superhydrophobic surface is to use a combination of rough or even hierarchical micro- or nanostructures and low-surface-energy material as exemplified by the rich literature in this topic.^{11–20} Some superhydrophobic surfaces have been produced without utilizing low-surface-energy materials or coatings.^{21–23}

This work presents a new multifunctional coating with high broadband transmittance and superhydrophobicity. It consists of grass-like alumina²⁴ (GLA) and fluoropolymer (FP). GLA is a novel nanoporous coating reported recently and exhibits broadband and omnidirectional antireflective properties²⁴ that are due to its gradient refractive index profile, which are known

to provide broadband and omnidirectional antireflection.^{25–28} The fluoropolymer is applied on top of GLA and serves as a low-surface-energy layer. The developed coating is superhydrophobic and effectively reduces reflection on glass and other materials with similar ($n \approx 1.5$) refractive index.

2. EXPERIMENTAL DETAILS

Substrate materials used in this work were 2 in.-diameter and 500 μm -thick soda lime glass wafers from UniversityWafer paired with silicon chips for characterization. Pairs of glass wafers and silicon chips underwent the same process steps simultaneously.

The fabrication process flow for the hydrophobic antireflective coating is outlined in Figure 1. The first step is atomic layer deposition (ALD) of Al_2O_3 to get a conformal flat film on the sample surface.²⁹ Deposition was performed in a Beneq TFS-500 reactor at 120°C using trimethylaluminum and water as precursors and run for 313 cycles. This process generally produces thin films with thickness of ca. 28 nm and refractive index $n \approx 1.64$, both from ellipsometry (He-Ne laser at 632.8 nm). The second step is immersion into deionized water (DIW), which transforms as-deposited Al_2O_3 into a porous, grass-like state.²⁴ The sample pairs (glass and silicon) were

Received: July 9, 2020

Accepted: October 7, 2020

Published: October 21, 2020



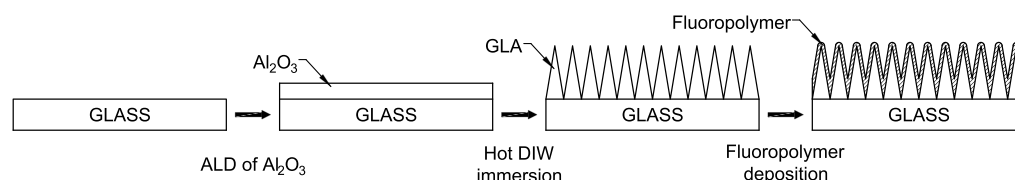


Figure 1. Fabrication process flow. First, a glass substrate is coated with ALD alumina. Then, grass-like alumina is formed by immersing the sample to hot DIW. Finally, the fluoropolymer is plasma-deposited on the grass-like alumina, resulting in a superhydrophobic antireflection coating. The fluoropolymer deposition time is varied, and all other parameters are fixed.

immersed into DIW heated up to 85–90 °C for 30 min. The DIW temperature was monitored with a thermocouple and stayed within the specified range. Further details on the grass-like alumina (GLA) fabrication and properties are described in detail elsewhere.²⁴ The obtained GLA coating has a rough surface with root-mean-square roughness of about 35 nm.²⁴ The last step is deposition of fluoropolymer as a low-surface-energy coating. The fluoropolymer was deposited in an RIE setup (model: Plasmalab 80Plus by Oxford Instruments); the deposition parameters are as follows: CHF₃ flow of 100 sccm at a pressure of 33.3 Pa (250 mTorr), RF power at 50 W, and substrate at room temperature. The thickness of the deposited fluoropolymer scales with deposition time; four sets of samples were prepared with 10, 7, 5, and 3 min fluoropolymer deposition times, and additional Si chips were added in each set for studying the deposition rate.

The measurements of transmittance were performed on a Cary 5000 UV–Vis–NIR spectrometer manufactured by Agilent. Thicknesses and refractive indices of the deposited coatings were measured by single wavelength (He-Ne laser at 632.8 nm) ellipsometry from the silicon chips as the measurement is much easier from opaque substrates and the surface chemistry of the native oxide-covered silicon is extremely similar to glass. Dynamic contact angle (DCA) measurements were taken using a Theta Optical Tensiometer from Biolin Scientific. DIW was used as the testing liquid and dynamic contact angles were obtained by pumping DIW in and then out of a droplet placed on the target surface. The droplet had a starting volume of 2 μL , and the advancing contact angle was retrieved while pumping in at a rate of 0.1 $\mu\text{L s}^{-1}$ for 50 s; right after that, the water was pumped out at a rate of 0.1 $\mu\text{L s}^{-1}$ for 70 s to retrieve the receding contact angle. Scanning electron microscopy (SEM) images were obtained using a Zeiss Supra 40 field-emission scanning electron microscope. Ellipsometric (five-point average) and DCA (three-point average) measurements as well as SEM images were taken from coatings on silicon chips; transmittance measurements were taken from coated soda lime glass wafers. Supplementary measurements confirmed that similarly prepared coatings on glass and silicon substrates produce consistent DCA results.

3. RESULTS AND DISCUSSION

The results of ellipsometric measurements after GLA formation and after subsequent fluoropolymer deposition are summarized in Table 1.

All samples experienced the same treatment until and including GLA formation, and the GLA thickness and

Table 1. Thickness (d) and Refractive Index (n) of the Coatings Obtained by Ellipsometry before and after Fluoropolymer Deposition

GLA		FP dep. time	GLA + FP	
d (nm)	n		d (nm)	n
129.2	1.187	3 min	139.7	1.212
129.0	1.186	5 min	152.7	1.212
129.1	1.186	7 min	165.2	1.213
131.2	1.186	10 min	191.2	1.215

refractive index are roughly the same in all samples, as expected. The standard deviation in thickness is only 1 nm, or 0.8%, and <0.1% in refractive index; these results are consistent with the previous literature.²⁴ After the fluoropolymer depositions, the refractive index of the composite coatings appears to be higher than that of GLA; this is expected because the fluoropolymer partially fills the voids in the porous GLA structure. Both thickness and refractive index are larger in coatings with more fluoropolymer deposited. The thickness increase is less significant for samples with a smaller amount of fluoropolymer because a larger portion of the deposited material is spent on filling the pores in GLA. For the same reasons, refractive index increase is most pronounced in thinner samples, but after the pores in the GLA are filled, the index increase is marginal.

It has to be noted that the thickness and refractive index of GLA obtained by single wavelength ellipsometry are only approximate values, valuable from the practical point of view, as they allow comparing samples and show the optical properties of the coatings. However, these values do not reflect real thickness from the bottom (interface with the substrate) to the top (highest peaks of the rough surface) of the coating; the real thickness of the porous GLA, which can be seen in, e.g., SEM images, is higher.²⁴ In addition, the refractive index value reflects the average index, while in reality, it has a gradient vertical profile in GLA.²⁴ Regardless of the mentioned imperfections, values obtained by ellipsometry have been shown to be good predictors for the performance of the GLA antireflective coating;²⁴ thereupon, they are used in this work.

Fluoropolymer deposition rate was studied, in addition, on bare Si chips in the same deposition runs as the samples. These chips have been coated with 15.8, 32.2, 43.7, and 65.2 nm-thick films in 3, 5, 7, and 10 min-long processes, respectively, which indicates that the deposition rate is 6.1 ± 0.6 nm/min. The thickness increase in the samples (see Table 1) is 5–9 nm lower than the fluoropolymer thickness on the reference chips. Given the porous and rough structure of GLA, fluoropolymer deposition, and the thickness measurement methodologies, such discrepancy is expected. A thicker fluoropolymer film was also produced on a 2" Si wafer to accurately measure the refractive index of the deposited fluoropolymer. With a deposition time of 30 min, the refractive index of the fluoropolymer thin film with ellipsometry was measured to be $n = 1.39$ and the resulting thickness was 181.5 nm (rate of 6.1 nm/min, the same as before). The $n = 1.39$ is quite comparable with values from the literature as the measured refractive index for polytetrafluoroethylene (PTFE) thin films is $n \approx 1.33$ –1.4 depending on the fabrication method and deposition parameters,^{30,31} and the dispersion in fluoropolymer films has been reported to be low in the visible region.³² The 181.5 nm-thick (30 min) film was also deposited on a 2"

glass wafer to study the absorption of the deposited FP. The measured absorption spectra (Figure S1) and a brief discussion are presented in the Supporting Information. The absorption of FP in the visible range is weak and mostly in the blue region; in addition, the FP thicknesses are a fraction (third or less) of the thick film, so transmittance losses are mainly due to reflection and/or scattering.

Table 2 shows advancing water contact angle (ACA) and receding water contact angle (RCA) measurements on glass

Table 2. Dynamic Contact Angles

sample	ACA	RCA	hysteresis
3 min FP	172.2°	<90°	
5 min FP	173.2°	160.1°	13.1°
7 min FP	172.6°	160.4°	12.2°
10 min FP	170.5°	148.0°	22.5°

coated with fluoropolymer-capped grass-like alumina. Samples with 5 and 7 min fluoropolymer deposition times exhibit the best superhydrophobic performance. The sample with 10 min fluoropolymer deposition time shows lower dynamic contact angles, which can be attributed to loss of roughness: the polymer deposited on top of GLA flattens the topographical features. GLA deposited with the parameters used in this work and a previous work²⁴ has surface roughness $R_q \approx 35$ nm and distance between pronounced features ranging from 20 to 200 nm. Considering this, adding extra ~ 65 nm (indicated by the reference Si chip, 10 min process) of coating on top of GLA will substantially alter the topography by hiding smaller features and blunting sharp peaks. As known from the literature,^{14–17} superhydrophobicity is strongly dependent on the rough topography of the coating. To verify the change in the topographical features of the GLA coated with FP of various thicknesses, cross-sectional SEM images of the prepared coatings have been made and are presented in Figure 2a–d. These images point out a continuous loss of sharpness in the surface features of the coatings: the 10 min FP

sample has the least sharp features compared to the other samples, which explains the loss of hydrophobicity. Sample with 3 min fluoropolymer deposition time had a favorable advancing contact angle, but the receding contact angle test showed hydrophilic behavior. This points to insufficient coverage by the fluoropolymer coating (pinholes)³³ and shows that the 3 min deposition time is too short. The geometry of features observed in Figure 2a is almost indistinguishable from the pure grass-like alumina reported previously,²⁴ which once again indicates very low thickness of the covering FP coating. It is important to note that the fluoropolymer conformally covers the complex topography of GLA, which is not unprecedented in a gas-phase deposition.

Fluoropolymer thin films plasma-deposited from pure CHF_3 gas have been used previously in microfluidics, for example, for droplet microfluidics on silicon requiring low surface energy³⁴ and as candidates for other microfluidics³⁵ or low-friction film studies.³¹ Previous work on fluoropolymer thin films plasma-deposited from pure CHF_3 indicates that very little hydrogen is present in the polymer as Fourier-transform infrared spectroscopy measurements were unable to detect C–H bonds,³⁶ and X-ray photoelectron spectroscopy (XPS) of fluoropolymer thin films plasma-deposited from pure CHF_3 using an RIE-tool with RF power under the substrate, like in this work, did not detect C–H bonds.³¹ Previous work also indicates from XPS a nonstoichiometric fluorine-to-carbon ratio ($\text{F}:\text{C} \approx 1.4\text{--}1.5$)³⁶ with excess carbon compared to an ideal polytetrafluoroethylene-like fluoropolymer made essentially from difluorocarbene (CF_2) with $\text{F}:\text{C} = 2$. The films are assumed to be cross-linked as XPS of fluoropolymer films made from pure CHF_3 and other pure fluorocarbon gases indicate that CHF_3 precursor films are cross-linked and have higher cross-linking than C_3F_8 precursor films; this enhanced cross-linking contributes to enhanced thermal stability.³⁷

A photo image of a droplet of water held by a needle on a surface of fluoropolymer-treated GLA (5 min sample) is presented in Figure 2e. As expected from a superhydrophobic surface, the water droplets do not adhere to the surface. In

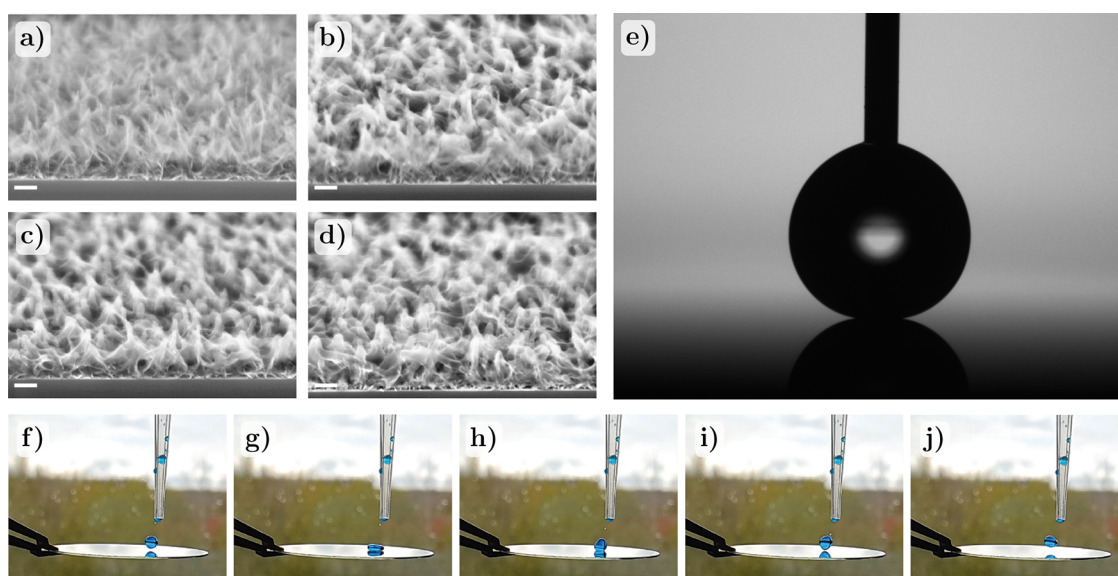


Figure 2. (a–d) Cross-sectional SEM images of Si coated with GLA and fluoropolymer, which was deposited for 3, 5, 7, and 10 min, respectively, and in the order of left to right; scale bars correspond to 100 nm. (e) Tensiometer image of a water droplet on fluoropolymer-coated (5 min) GLA. (f–j) Consecutive photos of a dyed water droplet falling onto a coated glass wafer and bouncing off it; the diameter of the wafer is 2 in.

addition, it was observed that a droplet falling onto this surface was bouncing off it, beautifully demonstrating water repellency. This process is demonstrated with consecutive photos of a dyed water droplet in Figure 2f–j and in a video supplied in the Supporting Information.

Results of transmittance measurements are displayed in Figure 3. The blue line with squares displays measured

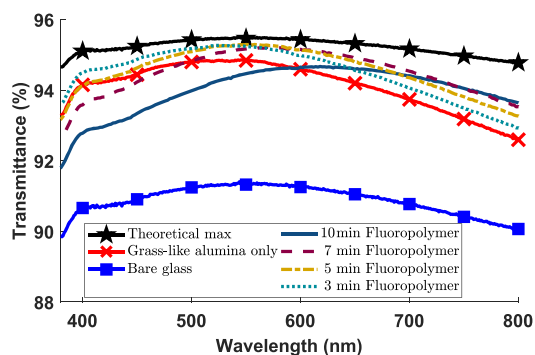


Figure 3. Transmittance measurements of uncoated glass, grass-like alumina (single-sided)-coated glass, and different fluoropolymer coatings on single-sided grass-like alumina-coated glass at normal incidence. The theoretical maximum for single-sided coated glass is equal to the transmittance for a half-plane of glass (semi-infinite), calculated from the transmittance of the bare glass wafer.

transmittance through an uncoated glass wafer. The black line with stars gives the theoretical maximum transmittance for single-sided coated glass wafer used in this work, which essentially is the transmittance out of a half-plane (semi-infinite) of the type of glass in question as then there is no front reflection. The theoretical maximum transmittance was calculated carefully from known data. The incidence angle is zero as in the measurements presented in Figure 3, which causes both polarizations to have the same reflectance at one interface

$$R_{12} = \frac{(n_2 - n_1)^2}{(n_2 + n_1)^2} \quad (1)$$

and

$$R_{12} = R_{21} \quad (2)$$

Furthermore, we assume that the coherence length of light is small enough that no interference effects occur, which is a reasonable assumption for nonlaser sources like black body sources, e.g., for sunlight³⁸ with a coherence length of ~600 nm,³⁹ especially given that the 500 μm -thick glass is well over a 100-fold thicker than this. The absorption in the bulk glass is negligible⁴⁰ and alumina is also very transparent in the visible spectrum,⁴¹ so we justifiably approximate absorption to zero; therefore

$$T = 1 - R \quad (3)$$

and

$$T_{12} = T_{21} \quad (4)$$

because of the normal incidence. With these conditions, the total transmittance through the glass slab is a geometric sum that yields

$$T_{\text{total}} = \frac{T_{\text{air-glass}} T_{\text{glass-air}}}{1 - R_{\text{glass-air}} R_{\text{glass-air}}} \quad (5)$$

From this, it can be derived that

$$T_{\text{glass-air}} = \frac{2T_{\text{total}}}{T_{\text{total}} + 1} \quad (6)$$

which is the theoretical maximum transmittance for single-sided coated glass and is identical to the transmittance out of a half-plane of glass (as now there is no front-side reflection because there is no front side).

The average transmittance through the glass in the visible range (defined as 400–700 nm) is 91.1% for uncoated glass, and 95.3% is the theoretical maximum transmittance for this glass type. The red line with crosses corresponds to the measured transmittance of single-sided GLA-coated glass wafer in which GLA was prepared in the same way as in the fluoropolymer-coated samples. This curve serves as a reference for the transmittance changes induced by fluoropolymer coatings, and the average transmittance in the visible range is 94.5%. The sample with the thickest fluoropolymer film (10 min sample, see Table 1) displayed a decrease in average transmittance down to 94.1% (compared to only GLA coating) and a significant red shift of peak transmittance. This shift is related to the destructive interference component of antireflective mechanisms in the structure, which is strongly dependent on the total thickness of the coating. In addition to the red shift in the 10 min FP sample, the transmittance is decreased because the gradient refractive index profile of GLA is compromised with a thicker fluoropolymer top coating. Other samples displayed increases in transmittance and negligible red shifts in peak transmittance: 3 and 5 min samples have average transmittance of 94.9%, and the 7 min sample has 94.7%; their peak transmittance almost reaches the theoretical maximum. Transmittance enhancement may be explained by the change in average refractive index of the structures (see Table 1), and samples with fluoropolymer have averaged indices of ~1.21, which closely match the optimal refractive index for an ARC at the air-glass interface

$$n_{\text{ARC}} = \sqrt{n_{\text{air}} n_{\text{glass}}} \approx 1.22 \quad (7)$$

These samples do not experience a decrease in transmittance because as we can estimate from Figure 2a–c, their gradient porosity profile, and hence gradient refractive index profile, is not severely compromised.

Overall, as shown in Figure 3, all samples have a substantial increase in transmittance (3–3.8%) compared to uncoated glass. Structures where the fluoropolymer was deposited for 3 and 5 min are the closest to the theoretical maximum in transmittance considering the visible spectral range. In applications where transmittance at 500 nm and above is more important, the 5 and 7 min samples exhibit superior transmittance; additionally, if we also consider superhydrophobic behavior (Table 2), then we can clearly conclude that the structures with 5 and 7 min fluoropolymer deposition times are the best performing as superhydrophobic antireflective coatings. Nevertheless, thicker top coating in 10 min samples might be advantageous in applications where better protection of porous GLA structure is required (although studies of coatings' robustness were not a part of this work).

4. CONCLUSIONS

This work has demonstrated a new superhydrophobic antireflective coating, which consists of grass-like alumina and plasma-deposited fluoropolymer. Grass-like alumina is deposited by atomic layer deposition of Al_2O_3 with subsequent immersion into heated deionized water; the fluoropolymer is deposited from CHF_3 plasma. The coating was able to increase the average transmittance from 91.1% (uncoated glass) to 94.9% (single-sided coated glass) while simultaneously demonstrating excellent superhydrophobic properties: 173° and 160° for advancing and receding water contact angles, respectively. It was found that 5 and 7 min-long fluoropolymer depositions produced the best results in terms of both superhydrophobicity and antireflection, while longer deposition, albeit showing lower transmittance, might be a better candidate in specific applications. Demonstrated multifunctional coating has very promising characteristics for solar energy, architectural glass, optical equipment, and other applications.

■ ASSOCIATED CONTENT

Supporting Information

The Supporting Information is available free of charge at <https://pubs.acs.org/doi/10.1021/acsami.0c12465>.

Absorption spectra of the glass and fluoropolymer (Figure S1) (PDF)

Video of water droplet falling onto glass wafer and bouncing off it (MP4)

■ AUTHOR INFORMATION

Corresponding Author

Kirill Isakov – Department of Electronics and Nanoengineering, Aalto University, FI-02150 Espoo, Finland; orcid.org/0000-0003-2380-2789; Email: kirill.isakov@aalto.fi

Authors

Christoffer Kauppinen – Department of Electronics and Nanoengineering, Aalto University, FI-02150 Espoo, Finland; orcid.org/0000-0002-2850-2702

Sami Franssila – Department of Chemistry and Materials Science and Micronova Nanofabrication Centre, Aalto University, FI-02150 Espoo, Finland

Harri Lipsanen – Department of Electronics and Nanoengineering, Aalto University, FI-02150 Espoo, Finland; orcid.org/0000-0003-2487-4645

Complete contact information is available at: <https://pubs.acs.org/10.1021/acsami.0c12465>

Notes

The authors declare the following competing financial interest(s): A patent application has been filed.

■ ACKNOWLEDGMENTS

The authors thank Business Finland (project: NANOGRA 6615/31/2019) for financial support and Academy of Finland (project: PREIN Flagship 320187). The authors recognize Micronova Nanofabrication Center and Nanomicroscopy Center at OtaNano, Aalto University for provision of facilities and technical support. The authors especially acknowledge Dr. Ville Jokinen for the advice on tensiometry.

■ REFERENCES

- (1) Sethi, S. K.; Manik, G. Recent Progress in Super Hydrophobic/Hydrophilic Self-Cleaning Surfaces for Various Industrial Applications: A Review. *Polym.-Plast. Technol. Eng.* **2018**, *57*, 1932–1952.
- (2) Ganesh, V. A.; Raut, H. K.; Nair, A. S.; Ramakrishna, S. A review on self-cleaning coatings. *J. Mater. Chem.* **2011**, *21*, 16304–16322.
- (3) Wisdom, K. M.; Watson, J. A.; Qu, X.; Liu, F.; Watson, G. S.; Chen, C.-H. Self-cleaning of superhydrophobic surfaces by self-propelled jumping condensate. *Proc. Nat. Acad. Sci.* **2013**, *110*, 7992–7997.
- (4) Mehmood, U.; Al-Sulaiman, F. A.; Yilbas, B. S.; Salhi, B.; Ahmed, S. H. A.; Hossain, M. K. Superhydrophobic surfaces with antireflection properties for solar applications: A critical review. *Sol. Energy Mater. Sol. Cells* **2016**, *157*, 604–623.
- (5) Zhang, Z. H.; Wang, H. J.; Liang, Y. H.; Li, X. J.; Ren, L. Q.; Cui, Z. Q.; Luo, C. One-step fabrication of robust superhydrophobic and superoleophilic surfaces with self-cleaning and oil/water separation function. *Sci. Rep.* **2018**, *8*, 3869.
- (6) Zhou, G.; He, J.; Gao, L.; Ren, T.; Li, T. Superhydrophobic self-cleaning antireflective coatings on Fresnel lenses by integrating hydrophilic solid and hydrophobic hollow silica nanoparticles. *RSC Adv.* **2013**, *3*, 21789–21796.
- (7) Nayshevsky, I.; Xu, Q.; Barahman, G.; Lyons, A. Anti-reflective and antisoiling properties of a KleanBoost™, a superhydrophobic nano-textured coating for solar glass. In *2017 IEEE 44th Photovoltaic Specialist Conference (PVSC)*; IEEE, 2017, pp. 2285–2290.
- (8) Zhou, S. Y.; Yang, B.; Li, Y.; Gao, X. R.; Ji, X.; Zhong, G. J.; Li, Z. M. Realization of ultra-high barrier to water vapor by 3D-interconnection of super-hydrophobic graphene layers in polylactide films. *J. Mater. Chem. A* **2017**, *5*, 14377–14386.
- (9) Zhang, F.; Chen, S.; Dong, L.; Lei, Y.; Liu, T.; Yin, Y. Preparation of superhydrophobic films on titanium as effective corrosion barriers. *Appl. Surf. Sci.* **2011**, *257*, 2587–2591.
- (10) Nine, M. J.; Cole, M. A.; Johnson, L.; Tran, D. N.; Losic, D. Robust Superhydrophobic Graphene-Based Composite Coatings with Self-Cleaning and Corrosion Barrier Properties. *ACS Appl. Mater. Interfaces* **2015**, *7*, 28482–28493.
- (11) Wenzel, R. N. Resistance of solid surfaces to wetting by water. *Ind. Eng. Chem.* **1936**, *28*, 988–994.
- (12) Cassie, A. B. D.; Baxter, S. Wettability of porous surfaces. *Trans. Faraday Soc.* **1944**, *40*, 546–551.
- (13) Onda, T.; Shibuichi, S.; Satoh, N.; Tsujii, K. Super-Water-Repellent Fractal Surfaces. *Langmuir* **1996**, *12*, 5–7.
- (14) Herminghaus, S. Roughness-induced non-wetting. *Europhys. Lett. (EPL)* **2000**, *52*, 165–170.
- (15) Öner, D.; McCarthy, T. J. Ultrahydrophobic surfaces. Effects of topography length scales on wettability. *Langmuir* **2000**, *16*, 7777–7782.
- (16) Yoshimitsu, Z.; Nakajima, A.; Watanabe, T.; Hashimoto, K. Effects of surface structure on the hydrophobicity and sliding behavior of water droplets. *Langmuir* **2002**, *18*, 5818–5822.
- (17) Bico, J.; Thiele, U.; Quéré, D. Wetting of textured surfaces. *Colloids Surf., A* **2002**, *206*, 41–46.
- (18) Song, Y.; Nair, R. P.; Zou, M.; Wang, Y. Superhydrophobic surfaces produced by applying a self-assembled monolayer to silicon micro/nano-textured surfaces. *Nano Res.* **2009**, *2*, 143–150.
- (19) Lim, H.; Jung, D. H.; Noh, J. H.; Choi, G. R.; Kim, W. D. Simple nanofabrication of a superhydrophobic and transparent biomimetic surface. *Chin. Sci. Bull.* **2009**, *54*, 3613–3616.
- (20) Yan, Y. Y.; Gao, N.; Barthlott, W. Mimicking natural superhydrophobic surfaces and grasping the wetting process: A review on recent progress in preparing superhydrophobic surfaces. *Adv. Colloid Interface Sci.* **2011**, *169*, 80–105.
- (21) Wang, J.; Liu, F.; Chen, H.; Chen, D. Superhydrophobic behavior achieved from hydrophilic surfaces. *Appl. Phys. Lett.* **2009**, *95*, 5–8.
- (22) Liu, T.; Kim, C.-J. Turning a surface superrepellent even to completely wetting liquids. *Science* **2014**, *346*, 1096–1100.

(23) Hoshian, S.; Jokinen, V.; Somerkivi, V.; Lokanathan, A. R.; Franssila, S. Robust superhydrophobic silicon without a low surface-energy hydrophobic coating. *ACS Appl. Mater. Interfaces* **2015**, *7*, 941–949.

(24) Kauppinen, C.; Isakov, K.; Sopanen, M. Grass-like Alumina with Low Refractive Index for Scalable, Broadband, Omnidirectional Antireflection Coatings on Glass Using Atomic Layer Deposition. *ACS Appl. Mater. Interfaces* **2017**, *9*, 15038–15043.

(25) Rayleigh, L. On Reflection of Vibrations at the Confines of two Media between which the Transition is Gradual. *Proc. London Math. Soc.* **1879**, *s1-11*, 51–56.

(26) Southwell, W. H. Gradient-Index Antireflection Coatings. *Opt. Lett.* **1983**, *8*, 584–586.

(27) Minot, M. J. Single-layer, gradient refractive index antireflection films effective from 0.35 to 2.5 μ . *J. Opt. Soc. Am.* **1976**, *66*, 515–519.

(28) Clapham, P. B.; Hutley, M. C. Reduction of Lens Reflexion by the "Moth Eye" Principle. *Nature* **1973**, *244*, 281–282.

(29) Puurunen, R. L. Surface chemistry of atomic layer deposition: A case study for the trimethylaluminum/water process. *J. Appl. Phys.* **2005**, *97*, 9.

(30) Prelipceanu, M.; Tudose, O.-G.; Prelipceanu, O.-S.; Schrader, S.; Grytsenko, K. Study of oriented growth of oligofluorene–thiophene films onto aligned vacuum-deposited polytetrafluoroethylene layers. *Mater. Sci. Semicond. Process.* **2007**, *10*, 24–35.

(31) Smith, B. K.; Brown, C. D.; LaVigne, G.; Sniegowski, J. J. Thin Teflon-like films for MEMS: film properties and reliability studies. In *Micromachining and Microfabrication Process Technology IV*; Society of Photo-Optical Instrumentation Engineers: 1998, 114–124.

(32) Gauch, M.; Ließmann, M.; Ehlers, H.; Ristau, D. Optical properties of fluorocarbon thin films prepared by ion beam sputtering of PTFE. In *Optical Interference Coatings*; Optical Society of America: 2013, p ThA.2.

(33) Law, K.-Y.; Zhao, H. *Non-wettable surfaces: theory, preparation and applications*; Ras, R. H.; Marmur, A., Eds.; Royal Society of Chemistry: 2016, p 178.

(34) Jokinen, V.; Sainiemi, L.; Franssila, S. Complex droplets on chemically modified silicon nanograss. *Adv. Mater.* **2008**, *20*, 3453–3456.

(35) Bayiati, P.; Tserepi, A.; Gogolides, E.; Misiakos, K. Selective plasma-induced deposition of fluorocarbon films on metal surfaces for actuation in microfluidics. *J. Vac. Sci. Technol., A* **2004**, *22*, 1546–1551.

(36) Winder, E. J.; Gleason, K. K. Growth and characterization of fluorocarbon thin films grown from trifluoromethane (CHF₃) using pulsed-plasma enhanced CVD. *J. Appl. Polym. Sci.* **2000**, *78*, 842–849.

(37) Astell-Burt, P. J.; Cairns, J. A.; Cheetham, A. K.; Hazel, R. M. A study of the deposition of polymeric material onto surfaces from fluorocarbon RF plasmas. *Plasma Chem. Plasma Process.* **1986**, *6*, 417–427.

(38) Abbot, C. The Sun's energy-spectrum and temperature. *Astrophys. J.* **1911**, *34*, 197.

(39) Donges, A. The coherence length of black-body radiation. *Eur. J. Phys.* **1998**, *19*, 245.

(40) Rubin, M. Optical properties of soda lime silica glasses. *Solar Energy Mater.* **1985**, *12*, 275–288.

(41) Aslan, M. M.; Webster, N. A.; Byard, C. L.; Pereira, M. B.; Hayes, C. M.; Wiederkehr, R. S.; Mendes, S. B. Lowloss optical waveguides for the near ultra-violet and visible spectral regions with Al₂O₃ thin films from atomic layer deposition. *Thin Solid Films* **2010**, *518*, 4935–4940.

NOTE ADDED AFTER ASAP PUBLICATION

This paper was published on the Web on October 21, 2020, with errors on the x-axis of the Table of Contents/Abstract graphic. The corrected version was reposted on October 21, 2020.